International Journal of Research and Review
[Indexed, Peer-Reviewed Journal]
Volume 13; Issue: 7; July 2026
Website: www.ijrrjournal.com
Research Paper *E-ISSN: 2349-9788; P-ISSN: 2454-2237*

Characterization of Energy Spectra and DNA Damage Induced by Secondary Electrons from Gadolinium Neutron Capture Therapy at Various Subcellular Locations Using Geant4-DNA and MCDS

Sri Hasniah Ashara[1], Catur Edi Widodo[2], Qidir Maulana Binu Soesanto[3]

[1]Department of Physics, Diponegoro University, Semarang, Indonesia.

Corresponding Author: Sri Hasniah Ashara

DOI: https://doi.org/10.52403/ijrr.20260725

ABSTRACT

This study characterized the energy spectra of secondary electrons reaching the nuclear surface and evaluated the resulting DNA damage from three different source locations: cell membrane, cytoplasm, and nucleus. Monte Carlo simulations were conducted using Geant4-DNA to model the isotropic emission of 10,000 secondary electrons from each compartment in a spherical cell geometry (nuclear radius = 3 μm). The energy spectra of electrons reaching the nuclear surface were subsequently analyzed for DNA damage using the Monte Carlo Damage Simulation (MCDS) code under normoxic conditions (21% O_2). Results showed that only 1.37% and 2.91% of electrons emitted from the cell membrane and cytoplasm, respectively, reached the nuclear surface, due to the very short range of Auger electrons (average energy 4.19 keV, range ≈ 12.5 nm). In contrast, higher-energy IC electrons (average 45.9 keV, range ≈ 38 μm) contributed significantly from peripheral locations. Nuclear localization produced the highest DNA damage, with double-strand break (DSB) yield increasing from 49.59 Gy^{-1} $cell^{-1}$ (cell membrane) to 50.16 Gy^{-1} $cell^{-1}$ (cytoplasm) and 53.27 Gy^{-1} $cell^{-1}$ (nucleus), representing a 7.41% enhancement. Complex lesions (DSB+, DSB++, DSBcb) were also significantly higher in the nucleus. Normalized per gigabase pair, the nuclear source yielded 8.87 DSBs Gy^{-1} Gbp^{-1}. These findings confirm that GdNCT efficacy strongly depends on the proximity of the source to nuclear DNA. The combination of Geant4-DNA and MCDS offers a reliable framework for predicting subcellular dose deposition and DNA damage complexity in GdNCT.

Keywords: *Neutron Capture Therapy, GdNCT, MCDS, Geant4-DNA*

INTRODUCTION

Cancer accounts for one in six deaths globally (16.8%) and one in four deaths (22.8%) from Noncommunicable Diseases (NCDs) worldwide[1]. Various therapeutic modalities have been developed, ranging from surgery, chemotherapy, radiotherapy, or combinations thereof[2]. Neutron Capture Therapy (NCT) has emerged as a promising approach for cancer treatment. It involves the use of specific isotopes that capture thermal neutrons, triggering nuclear reactions[3].

Gadolinium Neutron Capture Therapy (GdNCT) is a modality of NCT that utilizes the $^{157}Gd(n,\gamma)$ reaction, producing a cascade of low-energy secondary electrons, primarily Auger electrons and internal conversion (IC) electrons. These electrons have the potential to induce complex DNA damage in tumor cells[4]. The relative biological effectiveness (RBE) of these electrons is highly dependent on the spatial distribution of gadolinium within the cell[5]. The extremely short range of Auger electrons (~12.5 nm) limits energy deposition to the immediate vicinity of the neutron capture reaction site[6].

In the context of GdNCT, the characterization of the energy spectra of secondary electrons reaching the nuclear surface is a critical step in understanding subcellular dose deposition and the complexity of resulting DNA damage[5]. Auger electrons, with an average energy of approximately 4.19 keV and a range of ~12.5 nm, result in only a small fraction reaching the nuclear surface when emitted from the cell membrane or cytoplasm. In contrast, higher-energy IC electrons (average energy 45.9 keV, range ~38.19 μm) can contribute significantly to nuclear dose even when the gadolinium source is located at peripheral cellular sites[7][8].

Previous studies by Enger et al. (2013) and Golshani et al. (2021; 2022) demonstrated that although changes in RBE due to variations in gadolinium distribution are relatively small, the biological dose absorbed by DNA is highly sensitive to the position of gadolinium[9][10][11]. Despite this recognized biological potential, the majority of GdNCT studies to date have focused primarily on macroscopic dose calculations and RBE estimations at the tissue or organ level, assuming homogeneous gadolinium distribution. Explicit characterization of secondary electron energy spectra and their quantitative relationship with DNA damage yields at various subcellular locations remains limited in the GdNCT literature. Therefore, this study aims to characterize the energy spectra of secondary electrons reaching the nuclear surface and evaluate the resulting DNA damage induced from three different source locations: the cell membrane, cytoplasm, and nucleus.

This study employs a combined Monte Carlo simulation approach using Geant4-DNA and MCDS. Geant4-DNA, a specialized extension of the Geant4 platform developed by CERN, enables detailed simulation of electron transport in biological media down to energies below 1 eV, making it highly suitable for studying Auger and IC electrons from GdNCT[12]. Meanwhile, the Monte Carlo Damage Simulation (MCDS) code calculates the yields of DNA damage, including single-strand breaks (SSBs), double-strand breaks (DSBs), and complex lesions, based on the energy spectra of particles reaching the nucleus, while also accounting for the direct effects of oxygen concentration[13]. The two-stage approach combining Geant4-DNA and MCDS has proven computationally efficient and scientifically validated, as demonstrated by Qi et al. (2021) in their study of oxygen effects on DNA damage in BNCT[14].

MATERIALS & METHODS

Cellular Model

The cell geometry was modeled as a concentric three-compartment spherical structure representing a squamous cell carcinoma of the tongue with a total radius of 5 μm. The model consisted of three compartments, the outermost thin spherical surface representing the cell membrane (cytomembrane), the intermediate spherical shell representing the cytoplasm, and the innermost sphere representing the nucleus with a radius of 3 μm, which houses the cell's genetic material[14]. As illustrated in Figure 1, these three concentric components form a complete cell model. For computational simplicity, all cellular materials were defined as liquid water (G4_WATER) in the Geant4 simulation.

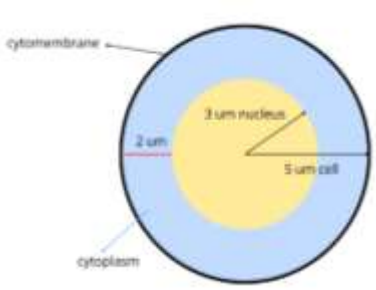

Figure 1. Cellular model.

Particle Transport Simulation Using Geant4-DNA

Geant4-DNA was employed to simulate the transport of secondary electrons generated from gadolinium neutron capture reactions within a biological cell model. The electromagnetic physics models selected for this simulation were G4EmDNAPhysics_option4 and G4EmStandardPhysics_option4, which are recommended models for accurate electron transport simulations in liquid water (a surrogate for biological tissue) over the energy range of 1 eV to 1 MeV[12]. Secondary electrons (both internal conversion and Auger electrons) were assumed to originate uniformly from three distinct subcellular compartments, in the nucleus, cytoplasm, and cell membrane. In each compartment, electrons were emitted isotropically. The combined energy spectrum of IC and Auger electrons served as the source distribution (Table 1).

Table 1. The emission spectra of IC and Auger electrons released during a 157GdNCT (Golshani et al., 2019)

Energy (Ev)	Prob.	Energy (Ev)	Prob.	Energy (Ev)	Prob.	Energy (Ev)	Prob.
1.E+00	0.4254	1.E+02	0.3237	1.E+04	0	1.E+06	0
2.E+00	0.0085	2.E+02	1.6890	2.E+04	0	2.E+06	0.0003
3. E+00	0	3. E+02	0.1320	3. E+04	0.2084	3. E+06	0
4. E+00	0	4. E+02	0.1118	4. E+04	0.0095	4. E+06	0
5. E+00	0	5. E+02	0.0365	5. E+04	0.0073	5. E+06	0
6. E+00	0	6. E+02	0.0223	6. E+04	0.0001	6. E+06	0
7. E+00	0	7. E+02	0.1074	7. E+04	0.0004	7. E+06	0
8. E+00	0	8. E+02	0.1894	8. E+04	0.4227	8. E+06	0
9. E+00	0	9. E+02	0.2343	9. E+04	0	9. E+06	0
1.E+01	0	1.E+03	0.1601	1.E+05	0		
2.E+01	0.0714	2.E+03	0.3142	2.E+05	0.0566		
3. E+01	0.0066	3. E+03	0	3. E+05	0.0009		
4. E+01	0.0646	4. E+03	0.0102	4. E+05	0		
5. E+01	0.0382	5. E+03	0.2368	5. E+05	0.0002		
6. E+01	0.0208	6. E+03	0.1732	6. E+05	0.0001		
7. E+01	0.1306	7. E+03	0.0428	7. E+05	0.0001		
8. E+01	0.1071	8. E+03	0.0037	8. E+05	0.001		
9. E+01	0.2738	9. E+03	0	9. E+05	0.004		

Particle Transport Simulation Using Geant4-DNA

The Monte Carlo Damage Simulation (MCDS 3.10A) code was used to calculate DNA damage yields based on the secondary electron energy spectra obtained from Geant4-DNA simulations. Employing MCDS as a standalone tool for DNA damage calculation offers significantly higher computational efficiency while maintaining sufficient accuracy for radiobiological analysis. The code has been extensively validated against experimental data for various radiation types, including photons, electrons, protons, and heavy ions. In this study, the total DNA content in the nucleus was set to 6 Gbp, which is representative of mammalian cells[15].

RESULT

Secondary electron transport to the nuclear surface

Geant4-DNA simulations were performed to evaluate the ability of secondary electrons from ^{157}GdNCT to reach the nuclear surface from three different subcellular

compartments. A total of 10,000 electrons were emitted isotropically and uniformly from each compartment. The number of electrons recorded at the nuclear surface (radius 3 μm) was 137 particles (1.37%) when emitted from the cell membrane (cytomembrane) and 291 particles (2.91%) when emitted from the cytoplasm. In contrast, when the source was located directly within the nucleus, 91.97% of the emitted electrons were recorded at the nuclear surface (kinetic energy recorded at the first simulation step immediately after emission). These differences clearly reflect the physical characteristics of the secondary electrons produced in GdNCT.

This phenomenon is predominantly governed by the characteristics of Auger electrons, which have an average energy of 4.19 keV and a very short range of approximately 12.5 nm in soft tissue[7]. Secondary electrons emitted from the cell membrane were almost entirely absorbed within the cytoplasm before reaching the nucleus. The distance between the cell membrane and the nuclear surface (~2 μm) greatly exceeds the range of Auger electrons, rendering their contribution to nuclear dose from the cell membrane negligible. Only the higher-energy internal conversion (IC) electrons, with an average energy of 45.9 keV and a range of approximately 38 μm, were able to contribute significantly from more distant cellular compartments[16].

This pattern is fully consistent with the principle proposed by Kassis (2004) that the therapeutic effect of Auger electrons is highly dependent on their proximity to DNA, as well as with the findings of Yu et al. (2024), who reported a similar gradient in DNA damage based on the subcellular distribution of gadolinium [8][17].

Effect of secondary electron distribution at different subcellular locations

Percentage of DNA Damage According to Complexity

Under normoxic conditions (21% O_2), the percentage of DNA damage clusters revealed that the nuclear source location produced a higher proportion of SSB, SSB+, 2SSB, and DSB compared to the cell membrane and cytoplasm. Figure 2(a) and (b) present the comparative percentages of DNA damage in the form of SSB and DSB. The percentage of SSB was highest in the nucleus (29.021%), followed by the cytoplasm (27.87%) and cell membrane (27.872%). A similar pattern was observed for DSB, with the nucleus showing higher percentages: 1.25% DSB, 0.198% DSB+, and 0.045% DSB++, compared to the cytoplasm and cell membrane. These results indicate that DNA damage not only increases quantitatively but also becomes more complex when the gadolinium source is located in the nucleus. In DNA damage, complex clustered lesions such as DSB+, DSB++, SSBcb, and DSBcb are biologically more difficult to repair and contribute significantly to cell death[18].

(a)

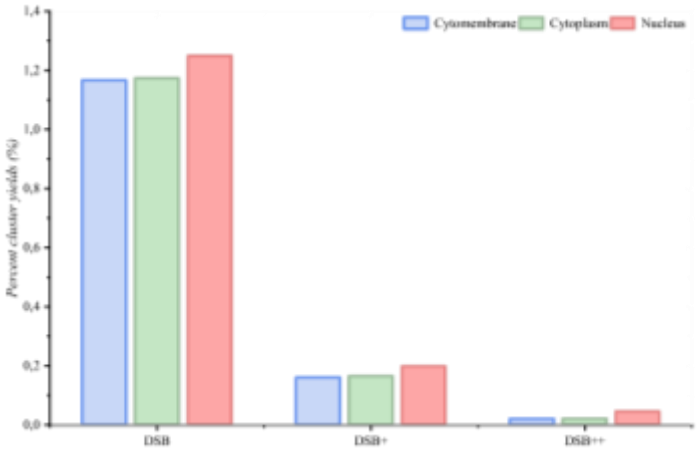

(b)

Figure 2. Percentage of DNA damage at different subcellular locations. (a) Complexity of single-strand breaks (SSB) and (b) complexity of double-strand breaks (DSB).

Table 2 presents the fractional distribution of various DNA damage types according to their complexity from the three source locations. Overall, simple damage types such as Base Damage (BD) and Single-Strand Breaks (SSB) dominated at all locations, with BD fractions ranging from 67.90% to 68.40% and SSB from 29.02% to 29.87%. However, the proportion of complex damage was consistently higher in the nucleus. Notably, the nucleus exhibited a higher fraction of complex DSBcb lesions, with an increase of 3.49% compared to the cell membrane and 3.52% compared to the cytoplasm. These findings support the hypothesis that short-range secondary electrons deposit energy most effectively at genomic targets when the gadolinium source is located within the cell nucleus.

Table 2. Percentage of DNA Damage Clusters by Complexity

Type	Cytomemb (%)	*Cytoplasm* (%)	*Nucleus* (%)	Δ Nuc–Memb	Δ Nuc–Cyto
BD	68,305	68,281	67,904	-0,401	-0,377
SSB	28,872	28,877	29,021	+0,149	+0,144
SSB+	1,312	1,318	1,503	+0,091	+0,085
2SSB	0,165	0,168	0,307	+0,042	+0,039
DSB	1,166	1,173	1,230	+0,064	+0,057
DSB+	0,159	0,164	0,192	+0,033	+0,028
DSB++	0,019	0,020	0,042	+0,023	+0,022
SSBc	4,869	4,892	5,256	+0,387	+0,364
SSBcb	40,786	40,899	42,192	+1,406	+1,293
DSBc	13,268	13,532	15,991	+2,723	+2,459
DSBcb	51,861	51,821	55,347	+3,486	+3,526

DNA damage yield per cell

In addition to analyzing the percentage of DNA damage, this study also quantified the absolute number of DNA lesions per cell, expressed in units of Gy^{-1} $cell^{-1}$. Consistent with the pattern shown in Figure 3, the number of double-strand breaks (DSBs) increased as the particle source was located closer to the DNA. The DSB yield was 49.59 Gy^{-1} $cell^{-1}$ when the source was in the cell membrane, increasing to 50.16 Gy^{-1} $cell^{-1}$ in the cytoplasm and reaching 53.27 Gy^{-1} $cell^{-1}$ in the nucleus. This corresponds to an overall enhancement of 7.41% in DSB yield. When the nuclear source DSB yield was normalized to DNA content using a conversion factor of 6 Gbp per mammalian cell (Ghosh and Jost, 2018), the value was 8.87 DSB Gy^{-1} Gbp^{-1}. This value exceeds the minimum of 8.63 ± 0.33 DSB Gy^{-1} Gbp^{-1} reported by Yu et al. (2024) as the lowest value across all conditions they

evaluated, and falls within the range reported in the literature for radiation with mixed linear energy transfer (LET) characteristics.

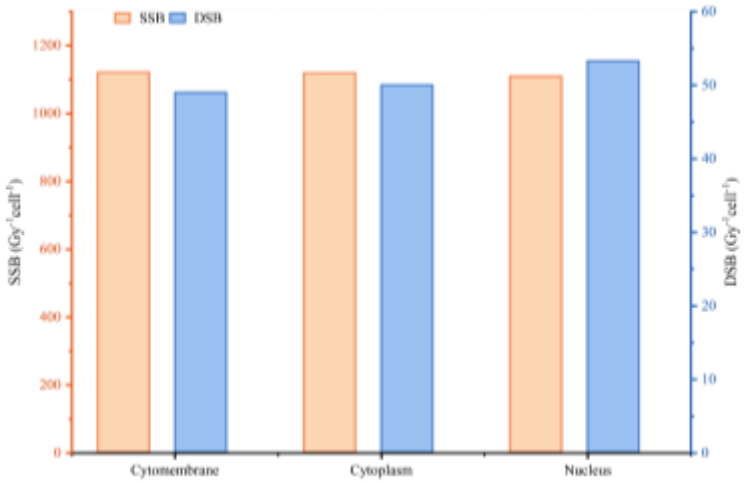

Figure 1. Number of clusters per cell ($Gy^{-1}Cell^{-1}$)

DISCUSSION

The present study demonstrates that the subcellular distribution of gadolinium significantly influences both the energy spectrum of secondary electrons reaching the nuclear surface and the resulting DNA damage complexity in GdNCT. Consistent with the very short range of Auger electrons (~12.5 nm), only 1.37% and 2.91% of electrons emitted from the cell membrane and cytoplasm, respectively, reached the nuclear surface. In contrast, higher-energy IC electrons (average 45.9 keV) contributed substantially even from peripheral locations. These findings align with previous Monte Carlo studies (Golshani et al., 2021; Yu et al., 2024) that highlighted the critical role of gadolinium localization in determining nuclear dose.

Quantitatively, the DSB yield increased from 49.59 Gy^{-1} $cell^{-1}$ (cell membrane) to 53.27 Gy^{-1} $cell^{-1}$ (nucleus), representing a 7.41% enhancement. When normalized per gigabase pair, the nuclear source yielded 8.87 DSB Gy^{-1} Gbp^{-1}, which exceeds the lowest value reported by Yu et al. (2024). More importantly, the proportion of complex DNA lesions (DSB+, DSB++, and DSBcb) was markedly higher when gadolinium was localized in the nucleus. This observation supports the long-standing hypothesis by Kassis (2004) that Auger electron emitters exert maximal therapeutic effect only when positioned in close proximity to nuclear DNA.

While the enhancement in total DSB yield appears modest, the increase in clustered and complex lesions is biologically significant, as such damage is more difficult to repair and more likely to lead to cell death. This study therefore reinforces the importance of nucleus-targeting strategies in GdNCT development.

Some limitations should be acknowledged. The simulation employed a simplified spherical cell geometry and assumed uniform distribution within each compartment, which may not fully represent the heterogeneous distribution of gadolinium compounds in real biological systems. Additionally, this study focused solely on normoxic conditions; the influence of hypoxia, a common feature of solid tumors, requires further investigation. Despite these limitations, the combination of Geant4-DNA and MCDS proved to be a robust and computationally efficient framework for evaluating subcellular radiobiological effects. Future studies should incorporate more realistic nuclear chromatin structures and evaluate the biological consequences under varying oxygen concentrations to better predict clinical outcomes of GdNCT.

CONCLUSION

This study characterized the energy spectra of secondary electrons and the resulting DNA damage from GdNCT at different subcellular locations using Geant4-DNA and MCDS simulations. The results demonstrate that the biological effectiveness of GdNCT is strongly dependent on the proximity of gadolinium to nuclear DNA. Due to the ultra-short range of Auger electrons, only 1.37% and 2.91% of electrons emitted from the cell membrane and cytoplasm reached the nucleus, respectively. Direct nuclear localization yielded the highest DSB yield (53.27 Gy^{-1} $cell^{-1}$), representing a 7.41% increase compared to the cell membrane source, with a normalized value of 8.87 DSB Gy^{-1} Gbp^{-1}. Complex DNA lesions were also significantly higher in the nucleus. These findings confirm the critical importance of nucleus-targeting strategies in GdNCT. The combined Geant4-DNA and MCDS approach provides a reliable framework for evaluating subcellular radiobiological effects and supporting the future development of GdNCT.

Declaration by Authors

Acknowledgement: None
Source of Funding: None
Conflict of Interest: No conflicts of interest declared.

REFERENCES

1. Bray F, Laversanne M, Sung H, Ferlay J, Siegel RL, Soerjomataram I, Jemal A. Global cancer statistics 2022: GLOBOCAN estimates of incidence and mortality worldwide for 36 cancers in 185 countries. CA Cancer Journal Clinicians. 2024;74(3):229-263. https://doi.org/10.3322/caac.21834
2. Debela DT, Muzazu SG, Heraro KD, Ndalama MT, Mesele BW, Haile DC, Kitui SK, Manyazewal T. New approaches and procedures for cancer treatment: Current perspectives. SAGE Open Medicine 2021 12; 9:20503121211034366. https://doi.org/10.1177/20503121211034366
3. Wu F, Sun P, Guo X, Zhang Y, Meng X, Li X, Li J, Chen N, Pei P. Nanocarrier-driven neutron capture therapy: Strategies and perspectives. Acta Biomater 2025 203:78-93. https://doi.org/10.1016/j.actbio.2025.07.009
4. Duan D, Han Y, Tu Z, Guo H, Zhang Z, Shi Y, Li J, Sun Q, Chen J, Li Z, and Liu T. Gadolinium neutron capture reaction-induced nucleodynamic therapy potentiates antitumor immunity. *CCS Chemistry* 2023; 11:2589-2602. https://doi.org/10.31635/ccschem.023.202202488
5. Ho SL, Yue H, Tegafaw T, Ahmad MY, Liu S, Nam SW, Chang Y, Lee GH. Gadolinium Neutron Capture Therapy (GdNCT) Agents from Molecular to Nano: Current Status and Perspectives. ACS Omega. 2022 12;7(3):2533-2553. https://doi.org/10.1021/acsomega.1c06603
6. Van Delinder KW, Khan R, Gräfe JL. Radiobiological impact of gadolinium neutron capture from proton therapy and alternative neutron sources using TOPAS-nBio. Med Phys. 2021 48(7):4004-4016. https://doi.org/10.1002/mp.14928
7. De Stasio G, Rajesh D, Casalbore P, Daniels MJ, Erhardt RJ, Frazer BH, Wiese LM, Richter KL, Sonderegger BR, Gilbert B, Schaub S, Cannara RJ, Crawford JF, Gilles MK, Tyliszczak T, Fowler JF, Larocca LM, Howard SP, Mercanti D, Mehta MP, Pallini R. Are gadolinium contrast agents suitable for gadolinium neutron capture therapy? Neurol Res. 2005;27(4):387-98. https://doi.org/10.1179/016164105x17206
8. Yu W, Pang Y, Ji T, Lu P, Liang L, Hu C, Hu Z, Hong B, and Chen N. Assessing DNA damage and relative biological effectiveness of the secondary electrons in gadolinium neutron capture therapy using an adapted Geant4-DNA. Radiation Physics and Chemistry 2024;218; 111546. https://doi.org/10.1016/j.radphyschem.2024.111546
9. Enger SA, Giusti V, Fortin MA, Lundqvist H. Dosimetry for gadolinium neutron capture therapy (GdNCT). Radiat Measurements. 2013; 56:301–304. doi: 10.1016/j.radmeas.2013.05.009
10. Golshani M, Azadegan B, and Mowlavi AA. Microdosimetry calculations and estimation of the relative biological effectiveness of the low-energy electrons

released during Gd neutron capture reaction. Radiation Physics and Chemistry. 2013;188: 109585, https://doi.org/10.1016/j.radphyschem.2021.109585

11. Golshani M, Mowlavi AA, and Azadegan B. Gadolinium neutron capture therapy: Calculation of 157Gd kerma factor and a dosimetry study using MCNP Monte Carlo code. Radiat Phys Chem. 2022; 199:110234. https://doi.org/10.1016/j.radphyschem.2022.110155
12. Incerti S, Kyriakou I, Bernal MA, Bordage MC, Francis Z, Guatelli S, Ivanchenko V, Karamitros M, Lampe N, Lee SB, Meylan S, Min CH, Shin WG, Nieminen P, Sakata D, Tang N, Villagrasa C, Tran HN, Brown JMC. Geant4-DNA example applications for track structure simulations in liquid water: A report from the Geant4-DNA Project. Med Phys. 2018;45(8): e722-e739. https://doi.org/10.1002/mp.13048
13. Semenenko VA, Stewart RD, Ackerman EJ. Monte Carlo simulation of base and nucleotide excision repair of clustered DNA damage sites. I. Model properties and predicted trends. Radiat Res. 2005;164(2):180-93. https://doi.org/10.1667/rr3402
14. Qi J, Geng C, Tang X, Tian F, Han Y, Liu H, Liu Y, Bortolussi S, Guan F. Effect of spatial distribution of boron and oxygen concentration on DNA damage induced from boron neutron capture therapy using Monte Carlo simulations. Int J Radiat Biol. 2021;97(7):986-996. https://doi.org/10.1080/09553002.2021.1928785
15. Ghosh SK, Jost D. How epigenome drives chromatin folding and dynamics, insights from efficient coarse-grained models of chromosomes. PLoS Comput Biol. 2018; 29;14(5):e1006159. https://doi.org/10.1371/journal.pcbi.1006159
16. Golshani M, Mowlavi AA, and Azadegan B. Computational assessment of the cellular dosimetry and microdosimetry of the gadolinium electrons released during neutron capture therapy. Biomedical Physics & Engineering Express 2019;*5*(2):025031. Doi: 10.1088/2057-1976/aaec33
17. Kassis AI, The amazing world of auger electrons, Int J Radiat Biol, 2004;80(11-12):789-803. https://doi.org/10.1080/09553000400017663
18. Hada M, Georgakilas AG. Formation of clustered DNA damage after high-LET irradiation: a review. J Radiat Res. 2008;49(3):203-10. https://doi.org/10.1269/jrr.07123

How to cite this article: Sri Hasniah Ashara, Catur Edi Widodo, Qidir Maulana Binu Soesanto. Characterization of energy spectra and DNA damage induced by secondary electrons from gadolinium neutron capture therapy at various subcellular locations using Geant4-DNA and MCDS. *International Journal of Research and Review*. 2026; 13(7): 216-223. DOI: *https://doi.org/10.52403/ijrr.20260725*

******